Flight & Ground Testing Data Set for an Unmanned Aircraft: Great Planes Avistar Elite

Conference Paper · January 2020

DOI: 10.2514/6.2020-0780

4 authors, including:

Or Dantsker
University of Illinois, Urbana-Champaign
30 PUBLICATIONS **160** CITATIONS
SEE PROFILE

Moiz Vahora
University of Illinois, Urbana-Champaign
14 PUBLICATIONS **19** CITATIONS
SEE PROFILE

Renato Mancuso
Boston University
44 PUBLICATIONS **465** CITATIONS
SEE PROFILE

AIAA SciTech Forum
6-10 January 2020, Orlando, FL
AIAA Scitech 2020 Forum

10.2514/6.2020-0780

Flight & Ground Testing Data Set for an Unmanned Aircraft: Great Planes Avistar Elite

Or D. Dantsker* and Marco Caccamo †
Technical University of Munich, Garching, Germany

Moiz Vahora‡
University of Illinois at Urbana-Champaign, Urbana, IL 61801

Renato Mancuso§
Boston University, Boston, MA 02215

This paper presents a flight and ground testing data set for a trainer-type unmanned aircraft, a Great Planes Avistar Elite, which is in the series of aircraft data sets that are being published online and freely available as part of the Unmanned Aerial Vehicle Database (UAVDB). The Unmanned Aerial Vehicle Database is being continually expanded to include many aircraft as they are tested. This paper includes: flight testing data and ground measurement and testing results. The ground testing yielded 3D scanning geometry, computational tool models, moment of inertia values, and propeller performance. Flight testing results as well as testing and setup techniques are also be presented in this paper. Additionally, details regarding aircraft construction and instrumentation are provided.

Nomenclature

AVL	=	Athena Vortex Lattice	c	=	wing mean chord
CAD	=	computer aided design	m	=	aircraft mass
CFD	=	computational fluid dynamics	p, q, r	=	roll, pitch and yaw rotation rates
AHRS	=	attitude and heading reference system	S	=	wing area
DOF	=	degree of freedom	u, v, w	=	body-fixed true velocity
ESC	=	electronic speed controller	V	=	total speed
GPS	=	global positioning system	x, y, z	=	position in ENU coordinate system
IMU	=	inertial measurement unit			
PWM	=	pulse width modulation	α	=	angle-of-attack
Re	=	Reynolds number	β	=	sideslip angle
RC	=	radio control	ϕ, θ, ψ	=	roll, pitch and heading angles
UAV	=	unmanned aerial vehicle	ρ	=	density of air

a_x, a_y, a_z = body-axis translational acceleration

*Researcher, Department of Mechanical Engineering, or.dantsker@tum.de
†Professor, Department of Mechanical Engineering, mcaccamo@tum.de
‡Graduate Researcher, Department of Aerospace Engineering, AIAA Student Member. mvahor2@illinois.edu
§Assistant Professor, Department of Computer Science. rmancuso@bu.edu

I. Introduction

In the past several years, there has been a major increase in the popularity of unmanned aerial vehicles (UAVs) for research, military, commercial, and civilian applications. Part of this uptrend in UAV use includes increase in the research related to them. There have been UAVs used to study aerodynamic qualities,[1,2] especially in high angle-of-attack conditions.[3–5] Others have been used as testbeds to develop new control algorithms.[6–11] Additionally, some unmanned aircraft are used as low-cost stand-ins for experiments that are too risky or costly to perform on their full scale counterparts.[12–15] Yet other times, unmanned aircraft are developed to explore new aircraft configurations[16–19] or flight hardware.[20–22]

Development of a UAV platform takes several stages. First the airframe must be developed, which may involve design creation and construction, in the case with a custom design, or just construction, in the case of an already designed and pre-constructed commercial-off-the-shelf airframe (often a model aircraft kit). Next, instrumentation will follow a similar development route, depending on whether it is custom or commercial-off-the-shelf. Then comes ground testing, which may involve loads testing, moment of inertia measurement, and pre-flight combined systems testing. In summation, these stages become extremely costly in terms of resources as well as time. A research group may spend many months or possibly years to develop an aircraft, which may only be flight tested for a limited time.

This paper presents a flight and ground testing data set for a trainer-type unmanned aircraft, a Great Planes Avistar Elite, which can be seen in Figure 1. This is the second of a series of aircraft that are being published online and freely available as part of the Unmanned Aerial Vehicle Database[23] (UAVDB)[a].

Figure 1. The flight-ready instrumented Great Planes Avistar Elite.

[a]UAVDB is published online at www.uavdb.org and includes other aircraft such as a 26%-scale Cub Crafters CC11-100 Sport Cub S2.[23,24]

II. Aircraft Description

The Great Planes Avistar Elite is a commercially available model aircraft designed for radio control flight training.[25] Specifically, the aircraft has a fixed high-wing configuration and is primarily constructed from wood and plastic film covering. Given the aircraft's ease of construction and operation, robustness, and re-configurablity, it has made an excellent UAV research testbed.[26–32]

A. Aircraft Construction

The aircraft was constructed mainly following manufacturer recommendation with the exception of the propulsion system change and some small improvements to the control surface actuator linkages. The aircraft was originally designed intended to use a nitro internal combustion engine, however, the aircraft was adapted to use an electric propulsion system as it provides near constant performance, increased reliability, and low vibrations. Aircraft construction photos can be found in Figure 2.Airframe specifications can be found in Tables 1 and 2.

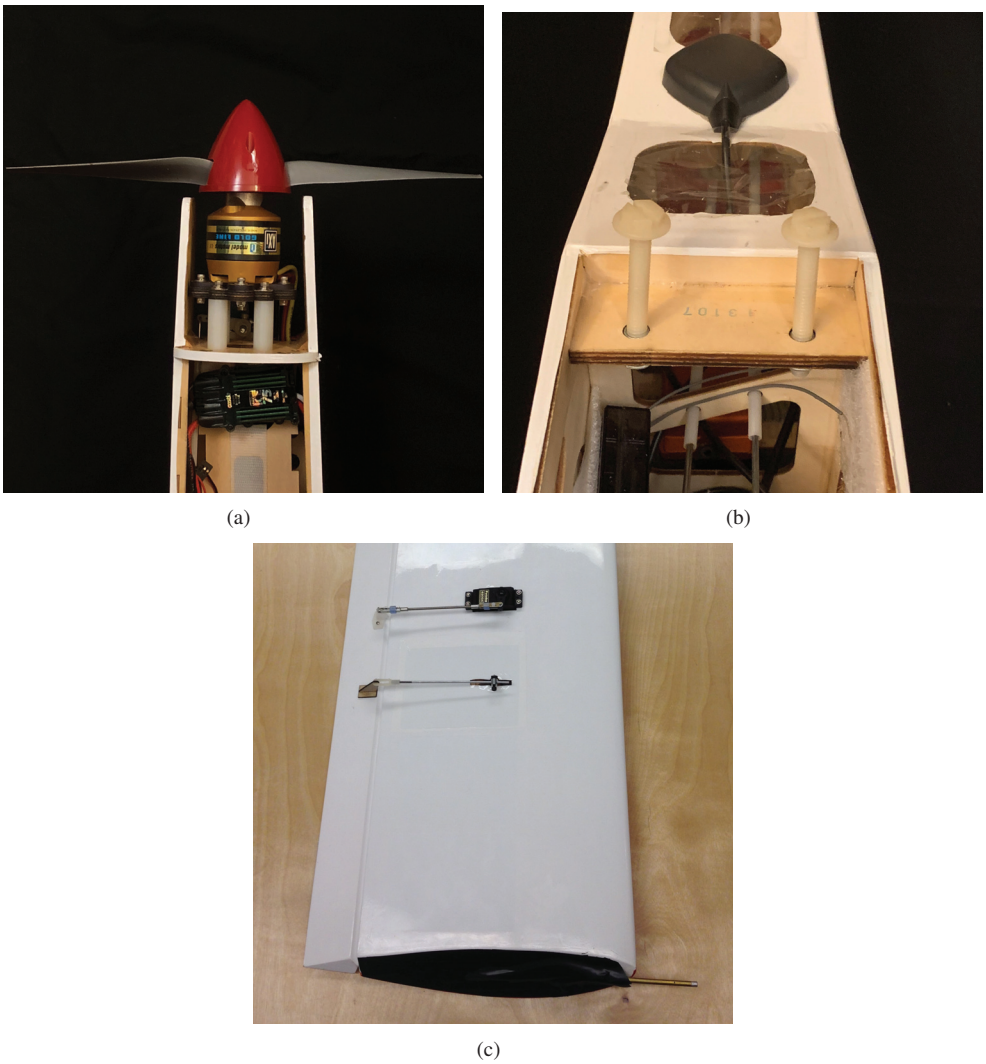

(a) (b)

(c)

Figure 2. Aircraft construction details: (a) nose of aircraft with brushless motor, propeller, and electronic speed controller (ESC), (b) rear of fuselage behind wing mounting location containing the inertial measurement unit (IMU) mounted inside and the GPS antenna ontop, and (c) outer wing with aileron servo and pitot probe.

Table 1. Airframe physical specifications.

Geometric Properties	
Overall Length	55.0 in (1395 mm)
Wing Span	62.5 in (1590 mm)
Wing Area	672 in^2 (43.3 dm^2)
Aspect Ratio	6.62
Inertial Properties	
Weight	
Empty (w/o Batteries)	3.77 lb (3.07 kg)
Batteries	1.39 lb (0.63 kg)
Gross Weight	8.16 lb (3.70 kg)
Wing Loading	28.0 oz/ft^2 (85.5 gr/dm^2)

Table 2. Airframe component specifications.

Construction	Built-up balsa and plywood structure, aluminum wing tube, aluminum landing gear, abs canopy, and plastic film sheeted.
Flight Controls	
Controls	Aileron (2), elevator, rudder, throttle, and flaps (2)
Transmitter	Futaba T14MZ
Receiver	Futaba R6014HS
Servos	(6) Futaba S3004
Regulator Distribution	Castle Creations CC BEC
Receiver Battery	Thunder ProLiteX 25c 2S 7.4V 450 mAh
Propulsion	
Motor	Model Motors AXI 4120/14 Outrunner
ESC	Castle Creation Phoenix Edge 75 Amp Brushless Speed Controller
Propeller	Landing Products APC 13x8E
Motor Flight Pack	Thunder Power ProLiteX 25c 4S 14.8 V 6 Ah lithium polymer battery
Flight Time	10-15 min

B. Instrumentation

The Avistar testbed aircraft was instrumented with an Al Volo FC+DAQ[33] data acquisition system. The system operates at 400 Hz and integrates with a 9 degree-of-freedom (9-DOF) XSens MTi-G-710[34] IMU with a GPS receiver. A pitot-static probe will be installed half-way down the span of the left wing in the near future. The pilot commands are also recorded by measuring the pulse width modulation (PWM) signals generated by receiver. The propulsion system information is logged by FDAQ through an interfaces with the Castle Creations ESC. Using the sensors, the system is able to log and transmit: 3D linear and angular accelerations, velocities, and position along with GPS location; pitot-static probe airspeed; 3D magnetic field strength and heading; control surface deflections; and motor voltage, current, RPM, and power. Specifications for the instrumentation can be found in Table 3.

Table 3. Instrumentation specifications.

Data acquisition system	Al Volo FC+DAQ 400 Hz system
Sensors	
Inertial measurement unit	XSens MTi-G-710 AHRS with GPS
Airspeed sensor	Al Volo Pitot Static Airspeed Sensor
Motor sensor	Al Volo Castle ESC Interface
Power	
Regulator	Built into FC+DAQ
Battery	Thunder Power ProLiteX 25c 3S 11.1 V 1350 mAh lithium polymer battery

III. Present Ground Measurement and Testing

To date, the Great Planes Avistar Elite aircraft has been extensively measured and ground tested using physical and simulated methods. This includes 3D scanning of the entire aircraft,[35] 3D modelling of the aircraft, generated models in several computational tools,[36] and moment of inertia testing.[29]

A. 3D Scanning

The 3D scanning was performed using a ZCorporation ZScanner 800 self-positioning handheld 3D scanner.[37] The 3D point cloud output from the scanner was processed using a previously written MATLAB script called AirplaneScan. The points on the right half of the airplane were discarded, and then the points on the left half were mirrored to the right with the exception of the nose gear, which was not mirrored.The resulting processed 3D point cloud can be seen in a 3-view and an isometric view in Fig. 3. The processed point cloud was then sliced multiple times to yield the cross sections of the fuselage, wings, and tail sections; the points were plotted in Figs. 4-7.

The pointcloud slices generated by the AirplaneScan MATLAB script provided dimensions and coordinates for all of the flight surfaces. It is important to note that the wing has the same airfoil along the wingspan and the empennage surfaces each have continuously varying airfoils from root to tip. The coordinates of each airfoil produced are plotted in Fig. 8. The wing airfoil coordinates were previously verified[35] with coordinates for the AVISTAR airfoil found on the UIUC Airfoil Database[38] and the stabilizer airfoils were verified with manual measurements. The dimensions of each flight surface and the airfoil locations are given in Table 4; the coordinate system used has the x-axis towards the tail, the y-axis towards the right wing, and the z-axis up. Using the fuselage geometry from the 3D scan and the aforementioned flight surface geometry, a computer aided design (CAD) model of the aircraft was modelled in SolidWorks (see Fig. 9).

Table 4. Avistar UAV flight surface specifications.

Wing							
LE x pos	**LE z pos**	**Incidence**	**y span pos**	**Chord**	**Offset**	**Dihedral**	**Airfoil**
380.4 mm	95.5 mm	3.58 deg	0 mm	237.10 mm	0 mm	0.9 deg	AVISTAR
-	-	-	793.75 mm	237.10 mm	0 mm	-	AVISTAR
Horizontal Stabilizer							
LE x pos	**LE z pos**	**Incidence**	**y span pos**	**Chord**	**Offset**	**Dihedral**	**Airfoil**
1160 mm	-2.04 mm	2.36 deg	0 mm	210 mm	0 mm	0 deg	AVISTARHSTABROOT
-	-	-	291 mm	110 mm	100 mm	-	AVISTARHSTABTIP
Vertical Stabilizer							
LE x pos	**LE z pos**	**Incidence**	**y span pos**	**Chord**	**Offset**	**Dihedral**	**Airfoil**
1160 mm	17.96 mm	2.36 deg	0 mm	273 mm	-95 mm	0 deg	AVISTARVSTABROOT
-	-	-	200 mm	96 mm	133 mm	-	AVISTARVSTABTIP

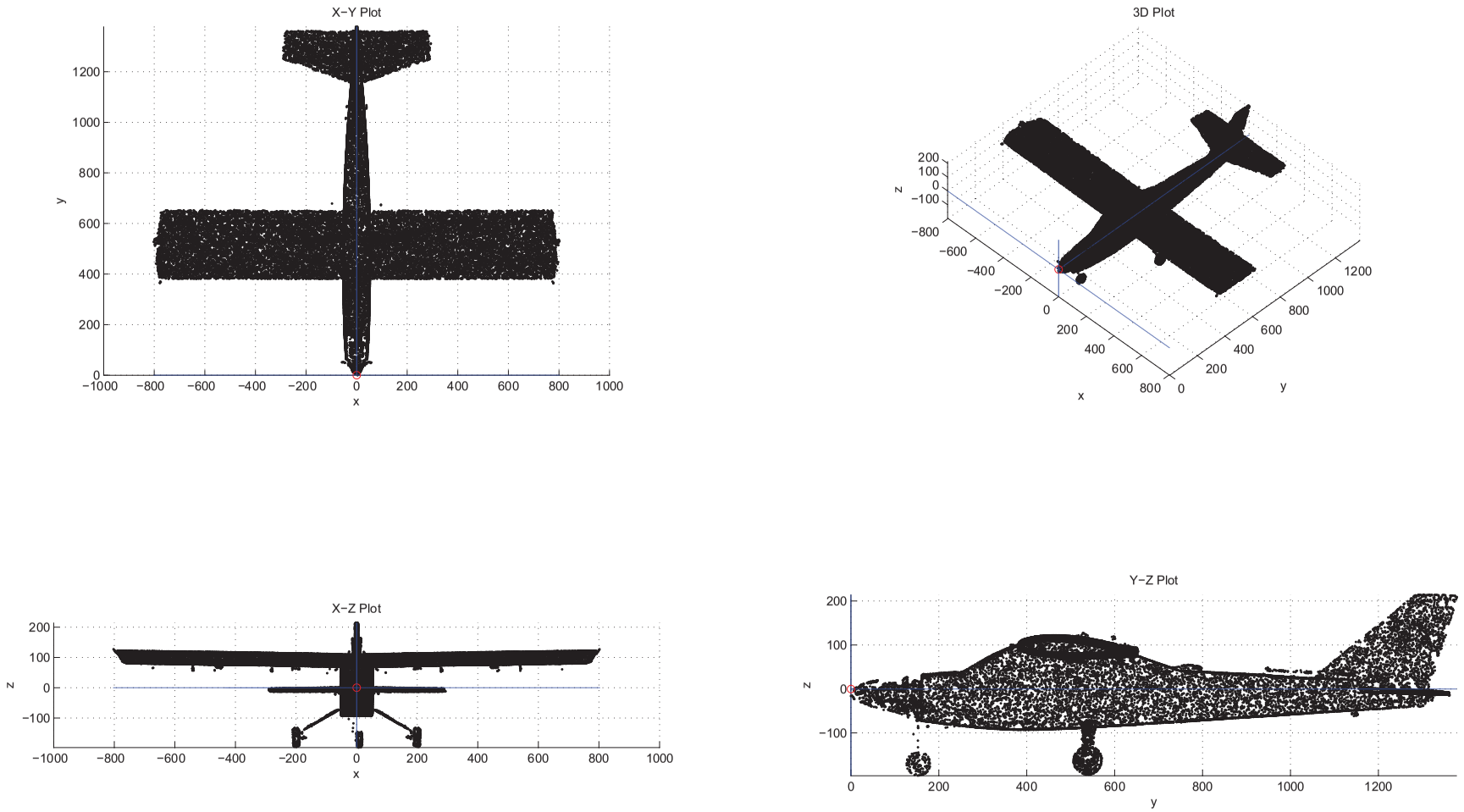

Figure 3. 3-view and isometric plots of the Avistar Elite scan after processing.

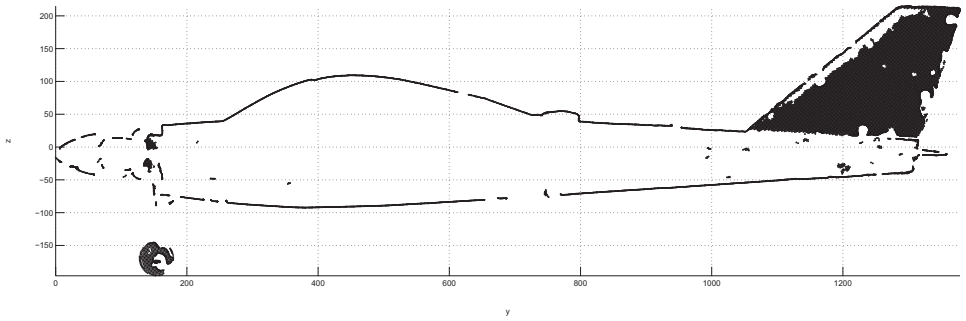

Figure 4. Plot of Y-Z slice of the 3D scan point cloud between x=-5 and x=5.

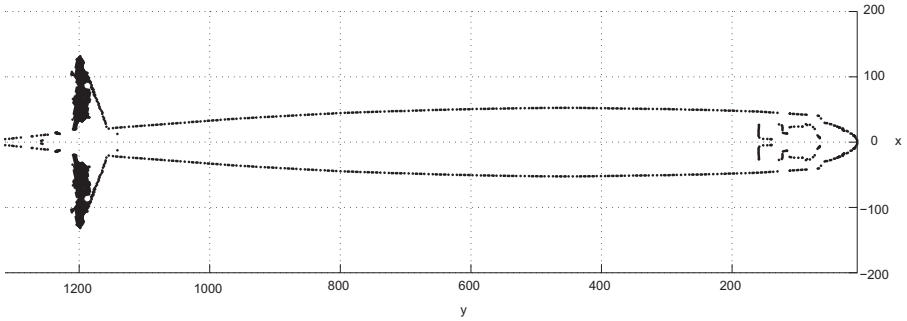

Figure 5. Plot of X-Y slice of the 3D scan point cloud between z=0 and z=1.

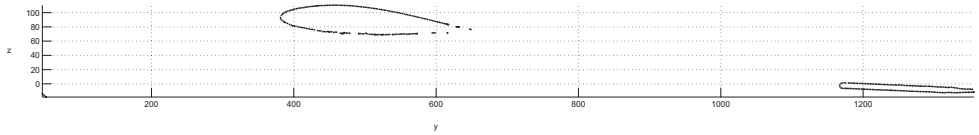

Figure 6. Plot of Y-Z slice of the 3D scan point cloud between x=53 and x=55.

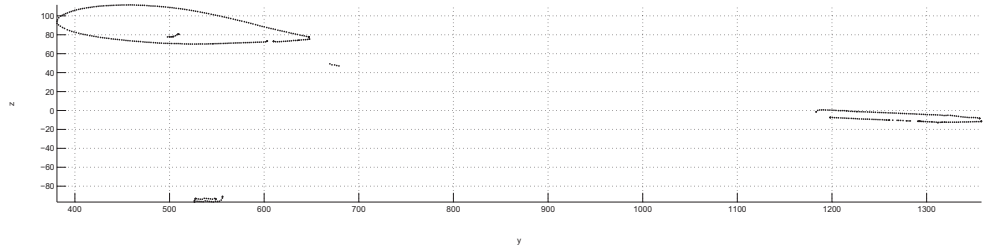

Figure 7. Plot of Y-Z slice of the 3D scan point cloud between x=98 and x=100.

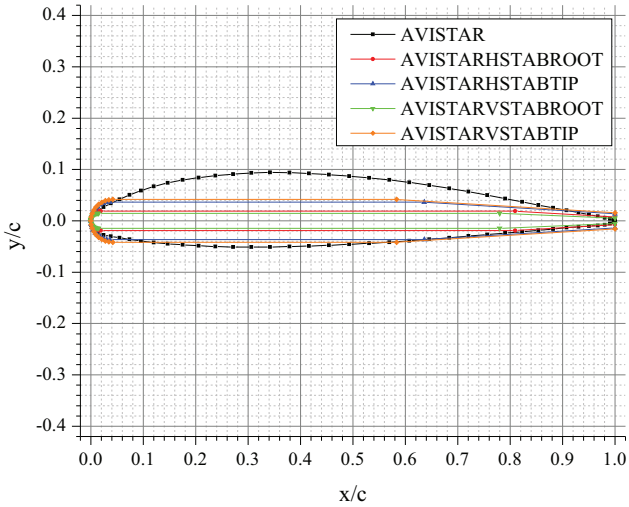

Figure 8. The airfoils used on the Avistar Elite.

Figure 9. A SolidWorks CAD model of the Avistar Elite.

B. Computational Tools

The 3D model of the Great Planes Avistar Elite generated using the point cloud was input into 2 types of computational tools. These computational tools make use of a vortex panel method solver to conduct aerodynamic analysis, consisting of XFLR5[39] and Athena Vortex Lattice (AVL).[40] Photos of the models are shown below in Figs. 10 and 11. These methods were used and compared to previous flight test campaigns with the Avistar Elite.[36] The models used to conduct the analysis are publicly available on the UAV database for additional analysis. Additionally the SolidWorks model of the Avistar generated from the point cloud is also available on the UAV database for integration in CFD solvers such as Ansys Fluent.

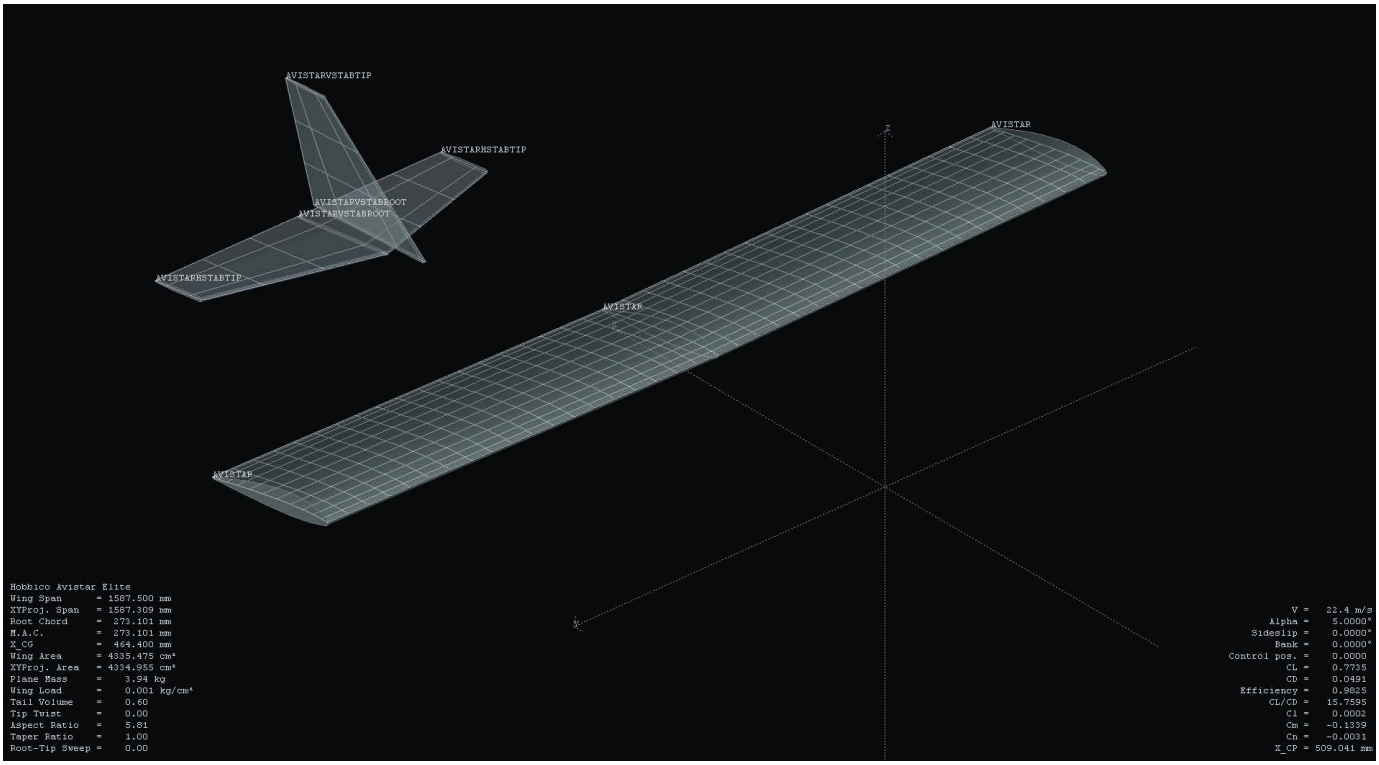

Figure 10. XFLR5 aerodynamics model for the Avistar UAV.

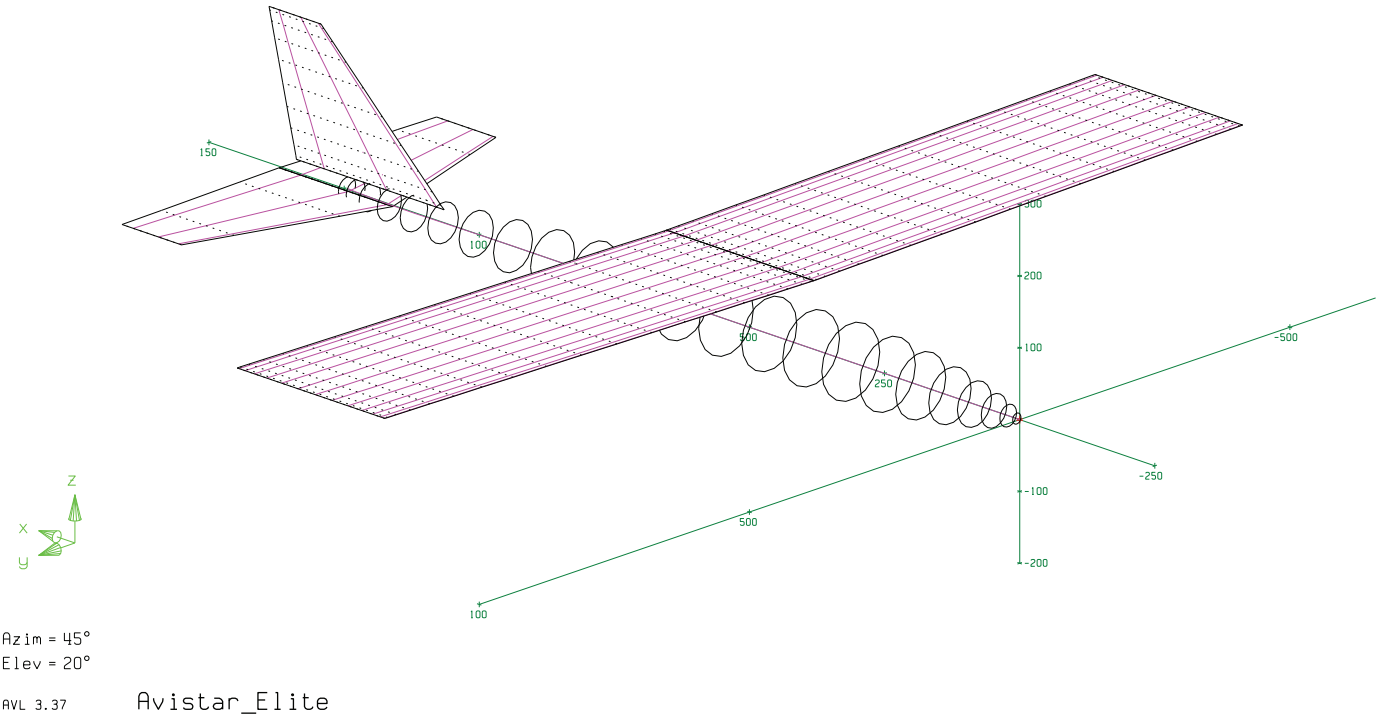

Figure 11. AVL aerodynamics model for the Avistar UAV.

C. Moment of Inertia Testing

Moment of inertia measurement of the flight-ready, instrumented Great Planes Avistar Elite aircraft was performed using a moment of inertia testing rig developed in previous work. A new mounting system was developed that hard mounts the aircraft to accurately measure values for all there axes. Note that due to the mounts, certain components, e.g. main landing gear, were tested separately, and that calibration of the mounts on their own is used to remove their inertia from the results. Photos of the testing are shown below in Fig. 12. Testing results, as well as raw data, can be found online on UAVDB. A thorough explanation of the process can be found in the previous literature.[29]

(a) (b)

(c)

Figure 12. Moment of inertia testing of the flight-ready, instrumented Great Planes Avistar Elite about the (a) roll axis, (b) pitch axis, and (c) yaw axis.

D. Propulsion System Testing and Modelling

The propulsion system on the Great Planes Avistar Elite consists of an Landing Products APC 13x8E propeller, Model Motors AXI 4120/14 brushless outrunner motor, Castle Creations Phoenix Edge 75 electronic speed controller, and a Thunder Power ProLiteX 25c 4-cell, 14.8 V 6 Ah lithium polymer battery. A propulsion system model of the propeller and motor, as well as a mission-based optimized list of possible motor-propeller combinations is found in previous literature.[31] Models of the ESC and battery can be found in other literature.[41–43]

Performance testing of the Landing Products APC 13x8E propeller, currently being used on the Great Planes Avistar Elite aircraft, as well as of several other propeller that could be used on the aircraft, will be performed in the UIUC low-turbulence subsonic wind tunnel using the equipment and procedures outlined in the literature.[44] Results of the testing will be published in a future publication[45] as well as on UAVDB and the UIUC Propeller Database[46]

IV. Flight Test Setup

The flight testing of the Great Planes Avistar Elite aircraft was conducted using the flight test automater developed by Dantsker et al.[47] The flight maneuvers that were performed by the aircraft using the flight test automater are detailed in Table 5; these maneuvers were selected as they are standard maneuvers for aircraft model system identification, i.e. singlets and doublets, and aerodynamic model development and validation, i.e. stalls and trimmed flight (level and gliding). The flight testing of the Avistar was conducted with a pilot and a operator. The pilot manually takes-off and lands the aircraft, as well as initially sets up the aircraft for automated flight, meanwhile, the operator monitors and commands the aircraft into preparatory holding patterns and the automated maneuvers using a ground station running uavEE.[48] In this setup, the pilot can override the autopilot at any time using the radio transmitter, in case of emergencies and for takeoff and landing. A screenshot of the ground station interface is shown in Fig. 13.

In order to conduct automated flight testing, and an initial trim maneuver needs to be performed. In this maneuver, the aircraft attempts to fly straight and level at a constant velocity within predefined steady-state noise bounds for a predefined amount of time; the control output values are averaged and the saved as trim, and used as the baseline for all maneuvers performed by the automator. For example, after an excitation (singlet or doublet), it is desired that the control surfaces be returned to trim such that the un-actuated response can be recorded. It should be noted that this maneuver requires low environmental disturbances (e.g. wind, thermals, etc).

Fig. 13 shows a screenshot of the uavEE ground station interface with the aircraft performing an up-down 1000 ms, 50% elevator deflection doublet maneuver. As shown in the figure, the aircraft is setup in a holding pattern the provides a consistent initial state before each maneuver. The aircraft is thus set up at the same speed and in approximately the same direction to ensure consistency. The direction of the pattern can be adjusted to accommodate for wind direction as to reduce cross wind effects, thus minimizing external β. As shown in Fig. 13, there is some crosswind present which causes each of the maneuvers paths to slightly deviate from the straight path it is set up on. It should be noted that the placement of the setup maneuver was also positioned to maintain line of sight throughout the experiments.

Table 5. Flight Test Maneuvers Planned

Maneuver	Variations	Description
Trimmed Flight	-	Straight and level flight at 20 m/s.
Idle Descent	-	Descent using idle power with trim for 20 m/s.
Stall	Vary aircraft weight	Starting with powered level flight at 20 m/s, the propulsion system is turned off, constant altitude is maintained until stall occurs, then centering of controls.
Aileron Singlet	Right or left, vary periods and amplitudes	Level flight followed by momentary aileron deflection and then centering of controls.
Aileron Doublet	Right-left or left-right, vary periods and amplitudes	Level flight followed by momentary aileron deflection in direction, then the other, and then centering of controls.
Elevator Singlet	Up or down, vary periods and amplitudes	Level flight followed by momentary aileron deflection and then centering of controls.
Elevator Doublet	Up-down or down-up, vary periods and amplitudes	Level flight followed by momentary aileron deflection in direction, then the other, and then centering of controls.
Rudder Doublet	Left-right or right-left, vary periods	Level flight followed by momentary aileron deflection in direction, then the other, and then centering of controls.

Figure 13. Screenshot of ground station interface with aircraft setup up for up-down 1000 ms, 50% elevator deflection doublet maneuver.

V. Results

The maneuvers outline in Table 5 were performed in the Fall of 2019. Each of these maneuvers were performed using the flight test automator functionality of uavAP and were repeated at least twice for each maneuver set. Using the flight test automator, each individual flight of 12-15 min allowed for approximately 20 maneuvers to be performed. There are minor differences between each of similar maneuver due to some factors such as initial aircraft state and external factors (e.g. wind). All time history and trajectory plots as well as flight data for the maneuvers performed are available on the UAVDB website. A subset of these maneuvers are presented in Fig. 14-31.

As mentioned in Section IV, flight testing starts with trim analysis, which is only required once per flight testing session (day). This maneuver is performed at 20 m/s and effectively yields straight and level flight, which can be seen in the trajectory plot shown in Fig. 15. Fig. 14 shows the time history of the maneuver with the aircraft at approximately steady state flight. The an idle decent maneuver is shown in Figs. 16 and 17. It should be noted that the aircraft is oriented in the wind direction, is trimmed at 20 m/s, and has 0 deg flap deflection (all of the maneuvers presented have 0 deg of flap).

Multiple stall maneuvers were conducted with the Avistar Elite at two different flight masses, the standard mass in Table 1 and at 250 g greater than that mass. The Avistar Elite tested at the greater mass was the testbed aircraft used to develop the flight test automator; it is of identical external geometry and very similar center of gravity position, however, contains additional electronics internally, causing the greater mass. The stall maneuver presented for both aircraft follows full scale testing whereby the maneuver starts with powered straight and level flight, then power is turned off and altitude is maintained with the use of elevator until the aircraft stalls. As can be seen in Figs. 18 and 19, the current testbed aircraft (used for all of the maneuvers presented except for Figs. 20 and 21) does not seem to exhibit stall with the allowed maximum elevator deflection applied gradually. Rather, the aircraft mushes and side-slips to the right at approximately 12 m/s. This finally ends when the elevator is centered, at which point the nose drops. However, with the heavier aircraft, the Avistar Elite design shows a visible stall, as can be seen in Figs. 20 and 21 at 5 s. The nose, i.e. pitch and angle of attack, drop after the aircraft reaches approximately 14 m/s, while the elevator is still held up.

The elevator is subsequently centered and recovery then occurs. It is important to note that these results were duplicated several times with each aircraft.

The control surface response for the ailerons, elevators, and rudder was then flight tested. Singlets and doublets were performed in each direction with varying periods and amplitudes for the ailerons and elevators. In a similar fashion, doublets were performed with the rudder. The maneuvers started with the aircraft in trimmed, straight and level flight. Once steady-state was reached, momentary deflections of the control surfaces were performed per Table 5. Aileron responses are shown in Figs. 26-29, elevator responses are shown in Figs. 22-25, and rudder responses are shown in Fig. 30 and 31. The results of these responses can be used to compute the aircraft control derivatives. Additionally, other aircraft behavior is visible. For example, in the rudder responses time history, it can be seen that the aircraft will roll as a result of rudder input and that the aircraft dampens quickly after the rudder is centered.

VI. Summary and Future Work

This flight and ground testing data sets were presented in this paper for the Great Planes Avistar Elite, which are being published on the Unmanned Aerial Vehicle Database. 3D scanning of the aircraft was performed, ultimately yielding an accurate CAD model of the aircraft as well as aircraft models for use in AVL, XFLR5, and for Fluent CFD analysis. Flight testing of the Avistar was then conducted with the use of a flight test automator. A subset of maneuvers were shown in this paper with the full data and figure set available on the UAVDB website.

The Unmanned Aerial Vehicle Database will be expanded to include additional aircraft as they are tested - including the Great Planes Avistar 30cc (an approximately 50% larger version of the Great Planes Avistar Elite presented in this paper) and a 22% scale Cessna 182 Skylane. Additionally, this data base will also include geometric and moment of inertia data sets for these aircraft, as well as propulsion system data sets and models.The flight testing of these aircraft will continue to be conducted using the flight testing automator, allowing for more consistent results.

Acknowledgments

The material presented in this paper is based upon work supported by the National Science Foundation (NSF) under grant number CNS-1646383. Marco Caccamo was also supported by an Alexander von Humboldt Professorship endowed by the German Federal Ministry of Education and Research. Any opinions, findings, and conclusions or recommendations expressed in this publication are those of the authors and do not necessarily reflect the views of the NSF.

Additionally, the authors would also like to thank Simon Yu for his help with flight testing. Finally, the authors owe thanks to Al Volo for their generous loan of data acquisition equipment.

References

[1]Lykins, R. and Keshmiri, S., "Modal Analysis of 1/3-Scale Yak-54 Aircraft Through Simulation and Flight Testing," AIAA Paper 2011-6443, AIAA Atmospheric Flight Mechanics Conference, Portland, Oregon, Aug. 2011.

[2]Johnson, B. and Lind, R., "Characterizing Wing Rock with Variations in Size and Configuration of Vertical Tail," *Journal of Aircraft*, Vol. 47, No. 2, 2010, pp. 567–576.

[3]Perry, J., Mohamed, A., Johnson, B., and Lind, R., "Estimating Angle of Attack and Sideslip Under High Dynamics on Small UAVs," Proceedings of the ION-GNSS Conference, Savannah, Georgia, 2008.

[4]Uhlig, D., Sareen, A., Sukumar, P., Rao, A. H., and Selig, M. S., "Determining Aerodynamic Characteristics of a Micro Air Vehicle Using Motion Tracking," AIAA Paper 2010-8416, AIAA Guidance, Navigation, and Control Conference, Toronto, Ontario, Canada, Aug. 2010.

[5]Dantsker, O. D. and Selig, M. S., "High Angle of Attack Flight of a Subscale Aerobatic Aircraft," AIAA Paper 2015-2568, AIAA Applied Aerodynamics Conference, Dallas, Texas, Jun. 2015.

[6]Mockli, M., *Guidance and Control for Aerobatic Maneuvers of an Unmanned Airplane*, Ph.D. thesis, ETH Zurich, Department of Mechanical and Process Engineering, 2006.

[7]Frank, A., McGrewy, J. S., Valentiz, M., Levinex, D., and How, J. P., "Hover, Transition, and Level Flight Control Design for a Single-Propeller Indoor Airplane," AIAA Paper 2007-6318, AIAA Guidance, Navigation, and Control Conference, Hilton Head, South Carolina, Aug. 2007.

[8]Johnson, E. N., Wu, A. D., Neidhoefer, J. C., Kannan, S. K., and Turbe, M. A., "Test Results of Autonomous Airplane Transitions Between Steady-Level and Hovering Flight," *Journal of Guidance, Control, and Dynamics*, Vol. 31, No. 2, 2008, pp. 358–370.

[9]Gaum, D. R., *Aggressive Flight Control Techniques for a Fixed-Wing Unmanned Aerial Vehicle*, Master's thesis, Stellenbosch University, Department of Electrical and Electronic Engineering, 2009.

[10]Bilodeau, P. R., Poulin, E., Gagnon, E., Wong, F., and Desbiens, A., "Control of a Hovering Mini Fixed Wing Aerial Vehicle," AIAA Paper 2009-5794, AIAA Guidance, Navigation and Control Conference, Chicago, Illinois, Aug. 2009.

[11]Johnson, B. and Lind, R., "Trajectory Planning for Sensing Effectiveness with High Angle-of-Attack Flight Capability," AIAA Paper 2012-0276, AIAA Aerospace Sciences Meeting, Nashville, Tennessee, Jan. 2012.

[12]Jordan, T. L. and Bailey, R. M., "NASA Langley's AirSTAR Testbed: A Subscale Flight Test Capability for Flight Dynamics and Control System Experiments," AIAA Paper 2008-6660, AIAA Atmospheric Flight Mechanics Conference, Honolulu, HI, Aug. 2008.

[13]Ragheb, A. M., Dantsker, O. D., and Selig, M. S., "Stall/Spin Flight Testing with a Subscale Aerobatic Aircraft," AIAA Paper 2013-2806, AIAA Applied Aerodynamics Conference, San Diego, CA, Jun. 2013.

[14]Bunge, R. A., Savino, F. M., and Kroo, I. M., "Approaches to Automatic Stall/Spin Detection Based on Small-Scale UAV Flight Testing," AIAA Paper 2015-2235, AIAA Atmospheric Flight Mechanics Conference, Dallas, Texas, Jun. 2015.

[15]Dantsker, O. D., Ananda, G. K., and Selig, M. S., "GA-USTAR Phase 1: Development and Flight Testing of the Baseline Upset and Stall Research Aircraft," AIAA Paper 2017-4078, AIAA Applied Aerodynamics Conference, Denver, Colorado, June 2017.

[16]Risch, T., Cosentino, G., Regan, C., Kisska, M., and Princen, N., "X-48B Flight-Test Progress Overview," AIAA Paper 2009-934, AIAA Aerospace Sciences Meeting, Orlando, FL, Jan. 2009.

[17]Lundstrom, D. and Amadori, K., "Raven: A Subscale Radio Controlled Business Jet Demonstrator," International Congress on the Aeronautical Sciences Systems (ICUAS), Anchorage, Alaska, Sep. 2008.

[18]Regan, C. D. and Taylor, B. R., "mAEWing1: Design, Build, Test - Invited," AIAA Paper 2016-1747, AIAA Atmospheric Flight Mechanics Conference, San Diego, California, Jun. 2016.

[19]Regan, C. D., "mAEWing2: Conceptual Design and System Test," AIAA Paper 2017-1391, AIAA Atmospheric Flight Mechanics Conference, Grapevine, Texas, Jun. 2017.

[20]Leong, H. I., Keshmiri, S., and Jager, R., "Evaluation of a COTS Autopilot and Avionics System for UAVs," AIAA Paper 2009-1963, AIAA Infotech@Aerospace, Seattle, Washington, April. 2009.

[21]Esposito, J. F. and Keshmiri, S., "Rapid Hardware Interfacing and Software Development for Embedded Devices Using Simulink," AIAA Paper 2010-3415, AIAA Infotech@Aerospace, Atlanta, Georgia, June 2010.

[22]Garcia, G. and Keshmiri, S., "Integrated Kalman Filter for a Flight Control System with Redundant Measurements," AIAA Paper 2012-2499, AIAA Infotech@Aerospace, Garden Grove, California, June 2012.

[23]O. D. Dantsker and R. Mancuso and M. Vahora and M. Caccamo, "Unmanned Aerial Vehicle Database," http://www.uavdb.org.

[24]O. D. Dantsker, M. V. and Mancuso, R., "Flight & Ground Testing Data Set for Subscale GA Aircraft: 26%-scale Cub Crafters CC11-100 Sport Cub S2," AIAA Paper 2019-1616, AIAA SciTech Forum, San Diego, California, Jan. 2019.

[25]Hobbico, Inc., "Great Planes Avistar Elite .46 Advanced Trainer RTF," http://www.greatplanes.com/airplanes/gpma1605.html, Accessed Oct. 2013.

[26]Mancuso, R., Dantsker, O. D., Caccamo, M., and Selig, M. S., "A Low-Power Architecture for High Frequency Sensor Acquisition in Many-DOF UAVs," Submitted to International Conference on Cyber-Physical Systems, Berlin, Germany, April 2014.

[27]Dantsker, O. D., Mancuso, R., Selig, M. S., and Caccamo, M., "High-Frequency Sensor Data Acquisition System (SDAC) for Flight Control and Aerodynamic Data Collection Research on Small to Mid-Sized UAVs," AIAA Paper 2014-2565, AIAA Applied Aerodynamics Conference, Atlanta, Georgia, June 2014.

[28]Dantsker, O. D., Loius, A. V., Mancuso, R., Caccamo, M., and Selig, M. S., "SDAC-UAS: A Sensor Data Acquisition Unmanned Aerial System for Flight Control and Aerodynamic Data Collection," *AIAA Infotech@Aerospace Conference, Kissimee, Florida, Jan 2015.*.

[29]Dantsker, O. D., Vahora, M., Imtiaz, S., and Caccamo, M., "High Fidelity Moment of Inertia Testing of Unmanned Aircraft," AIAA Paper 2018-4219, AIAA Applied Aerodynamics Conference, Atlanta, Georgia, Jun. 2018.

[30]Dantsker, O. D., Theile, M., and Caccamo, M., "A High-Fidelity, Low-Order Propulsion Power Model for Fixed-Wing Electric Unmanned Aircraft," AIAA/IEEE Electric Aircraft Technologies Symposium, Jul. 2018.

[31]Dantsker, O. D., Imtiaz, S., and Caccamo, M., "Electric Propulsion System Optimization for Long-Endurance and Solar-Powered Unmanned Aircraft," AIAA Paper 2019-4486, 2019 AIAA/IEEE Electric Aircraft Technologies Symposium, Indianapolis, Indiana, Aug. 2019.

[32]Theile, M., Yu, S., Dantsker, O. D., and Caccamo, M., "Trajectory Estimation for Geo-Fencing Applications on Small-Size Fixed-Wing UAVs," IEEE International Conference on Intelligent Robots and Systems, Macau, China, Nov. 2019.

[33]Al Volo LLC, "Al Volo: Flight Data Acquisition Systems," http://www.alvolo.us.

[34]Xsens Technologies B.V., "XSens, MTi-G-700," https://www.xsens.com/products/mti-g-700/, Accessed Jan. 2016.

[35]Dantsker, O. D., "Determining Aerodynamic Characteristics of an Unmanned Aerial Vehicle using a 3D Scanning Technique," AIAA Paper 2015-0026, AIAA Aerospace Sciences Meeting, Kissimmee, Florida, Jan. 2015.

[36]Dantsker, O. D. and Vahora, M., "Comparison of Aerodynamic Characterization Methods for Design of Unmanned Aerial Vehicles," AIAA Paper 2018-0272, AIAA Aerospace Sciences Meeting, Kissimmee, Florida, Jan 2018.

[37]ZCorporation, "The New ZScanner 800," www.zcorp.com/documents/182_ZScanner800-tearsheet-v05wb.pdf, Accessed Mar. 2013.

[38]UIUC Applied Aerodynamics Group, "UIUC Airfoil Coordinates Database," http://aerospace.illinois.edu/m-selig/ads/coord_database.html.

[39]Andre Deperrois, "XFLR5," http://www.xflr5.com/, Accessed Jun. 2017.

[40]Mark Drela, "AVL," http://web.mit.edu/drela/Public/web/avl/, Accessed Jun. 2017.

[41]Green, C. R. and McDonald, R. A., "Modeling and Test of the Eciency of Electronic Speed Controllers for Brushless DC Motors," AIAA Paper 2015-3191, AIAA Aviation Forum, Dallas, Texas, Jun. 2015.

[42]Gong, A. and Verstraete, D., "Experimental Testing of Electronic Speed Controllers for UAVs," AIAA Paper 2017-4955, AIAA/SAE/ASEE Joint Propulsion Conference, Atlanta, Georgia, July 2017.

[43]Gong, A., MacNeill, R., and Verstraete, D., "Performance Testing and Modeling of a Brushless DC Motor, Electronic Speed Controller and Propeller for a Small UAV," AIAA Paper 2018-4584, AIAA Propulsion and Energy Forum, Cincinnati, Ohio, July 2018.

[44]Brandt, J. B. and Selig, M. S., "Propeller Performance Data at Low Reynolds Numbers," AIAA Paper 2011-1255, AIAA Aerospace Sciences Meeting, Orlando, Florida, Jan. 2011.

[45]Dantsker, O. D., Caccamo, M., Deters, R. W., and Selig, M. S., "Performance Testing of Aero-Naut CAM Folding Propellers," Submitted to AIAA Applied Aerodynamics Conference, Reno, Nevada, Jun. 2020.

[46]UIUC Applied Aerodynamics Group, "UIUC Propeller Database," http://m-selig.ae.illinois.edu/props/propDB.html.

[47]O. D. Dantsker, S. Yu, M. V. and Caccamo, M., "Flight Testing Automation to Parameterize Unmanned Aircraft Dynamics," AIAA Paper 2019-3230, AIAA Aviation Forum, Dalllas, Texas, Jun. 2019.

[48]Theile, M., Dantsker, O. D., Nai, R., and Caccamo, M., "uavEE: A Modular, Power-Aware Emulation Environment for Rapid Prototyping and Testing of UAVs," Accepted to IEEE International Conference on Embedded and Real-Time Computing Systems and Applications, Hakodate, Japan, Aug. 2018.

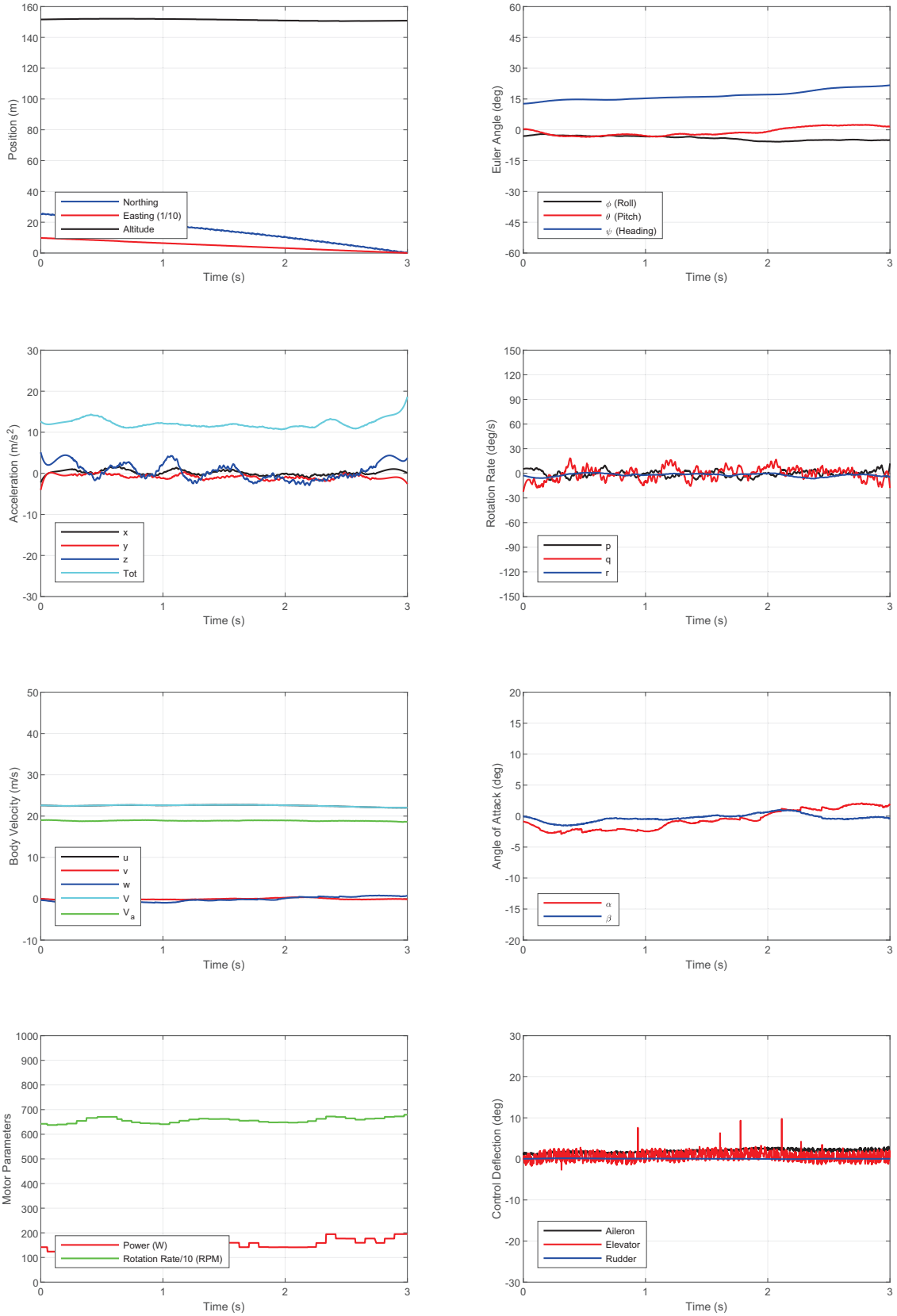

Figure 14. Time history of aircraft state during trimmed flight at 20m/s.

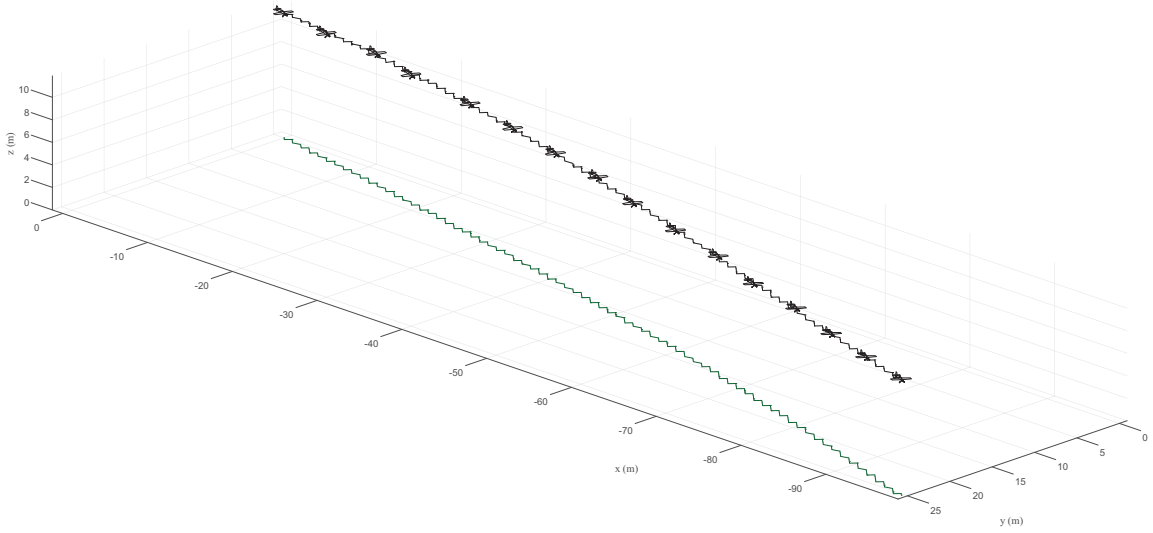

Figure 15. Trajectory of the aircraft during during trimmed flight at 20m/s (the aircraft is drawn once every 0.2 s).

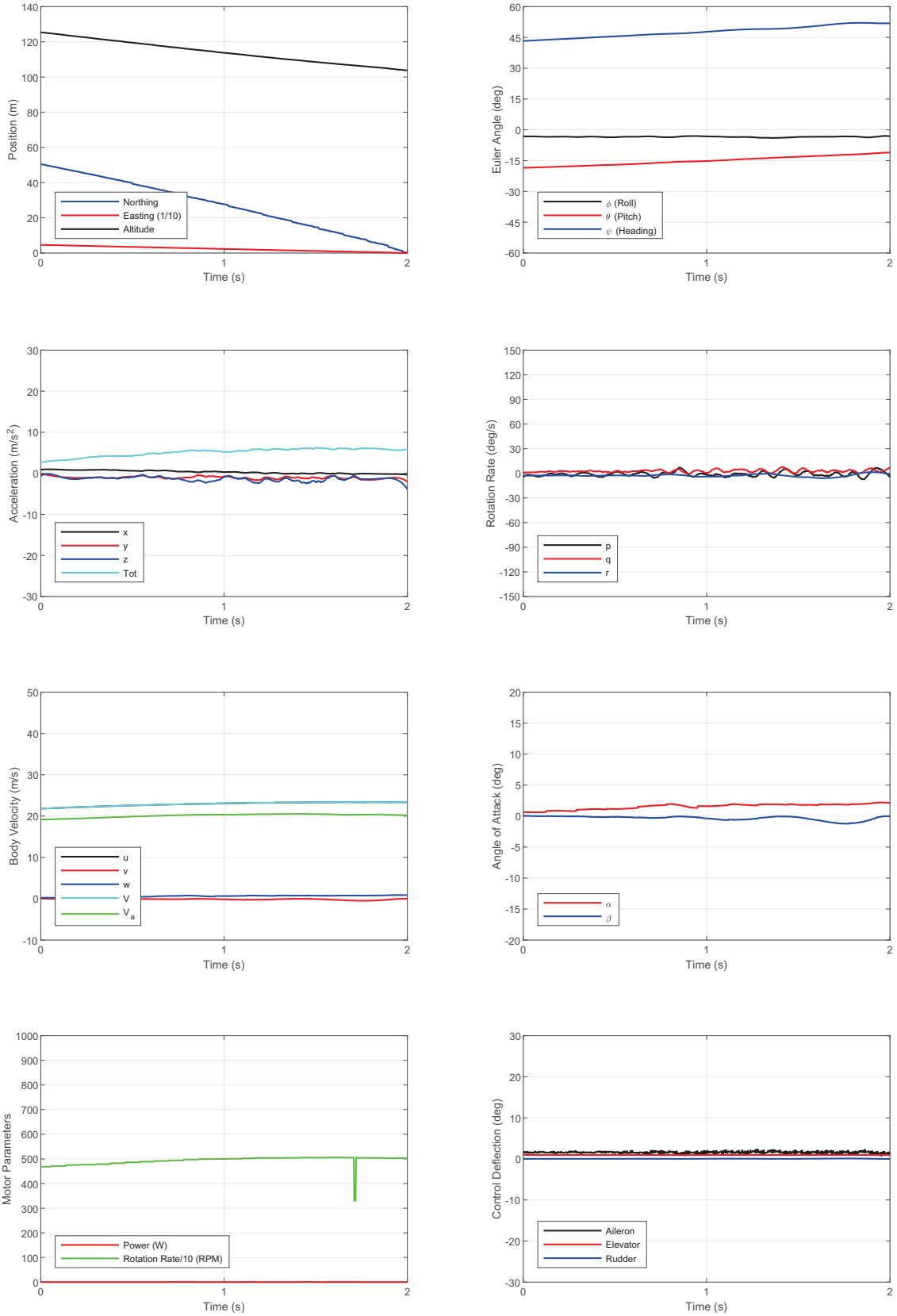

Figure 16. Time history of aircraft state during idle decent.

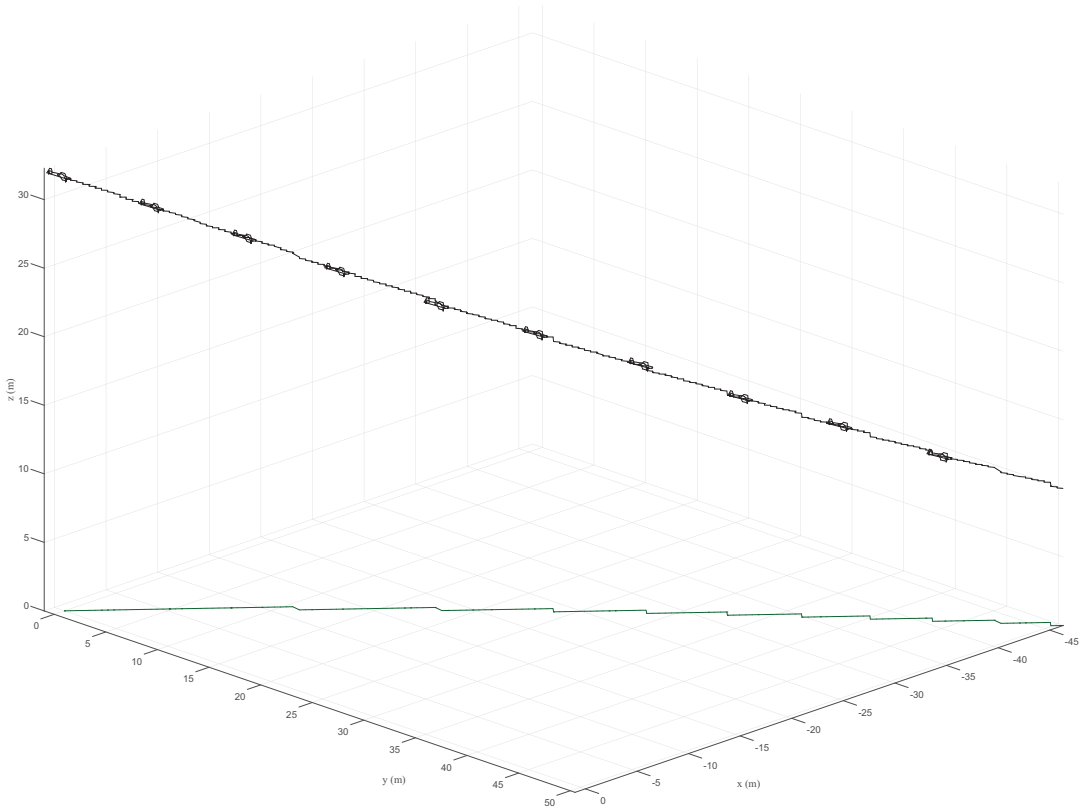

Figure 17. Trajectory of the aircraft during idle decent (the aircraft is drawn once every 0.2 s).

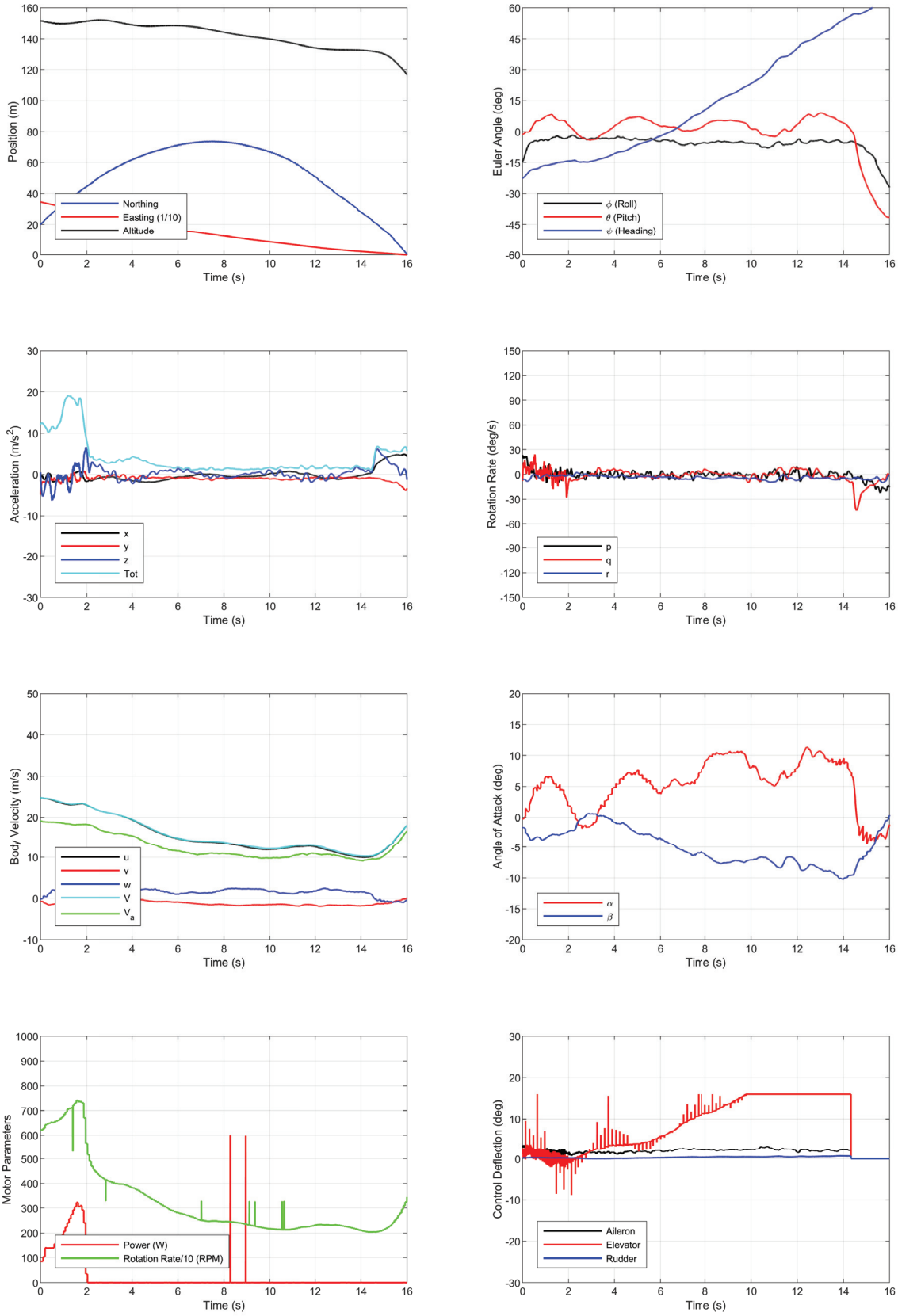

Figure 18. Time history of aircraft state during stall at standard mass.

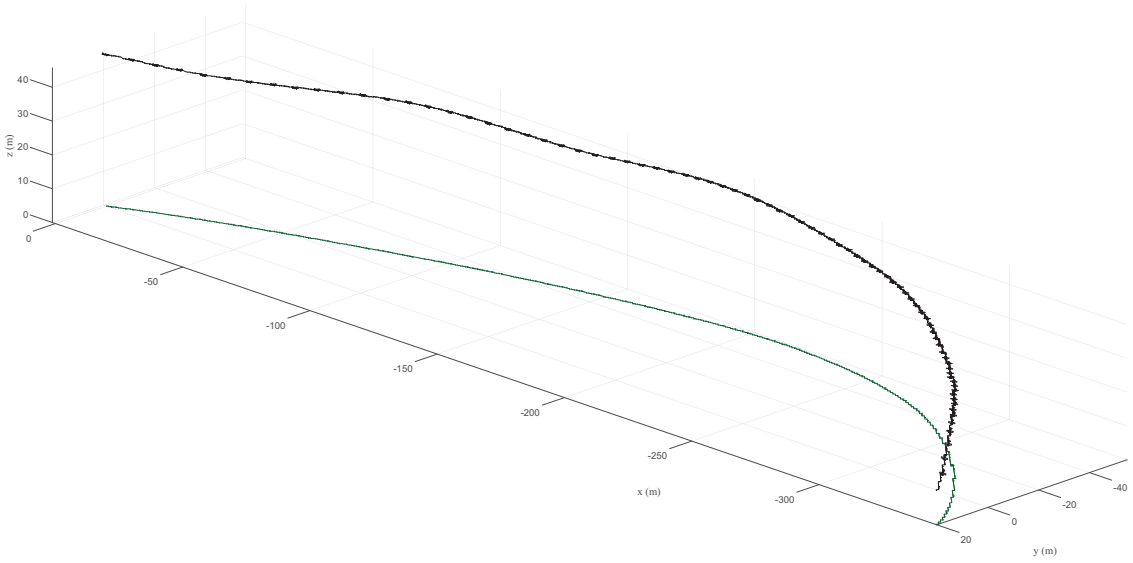

Figure 19. Trajectory of the aircraft during stall at standard mass (the aircraft is drawn once every 0.2 s).

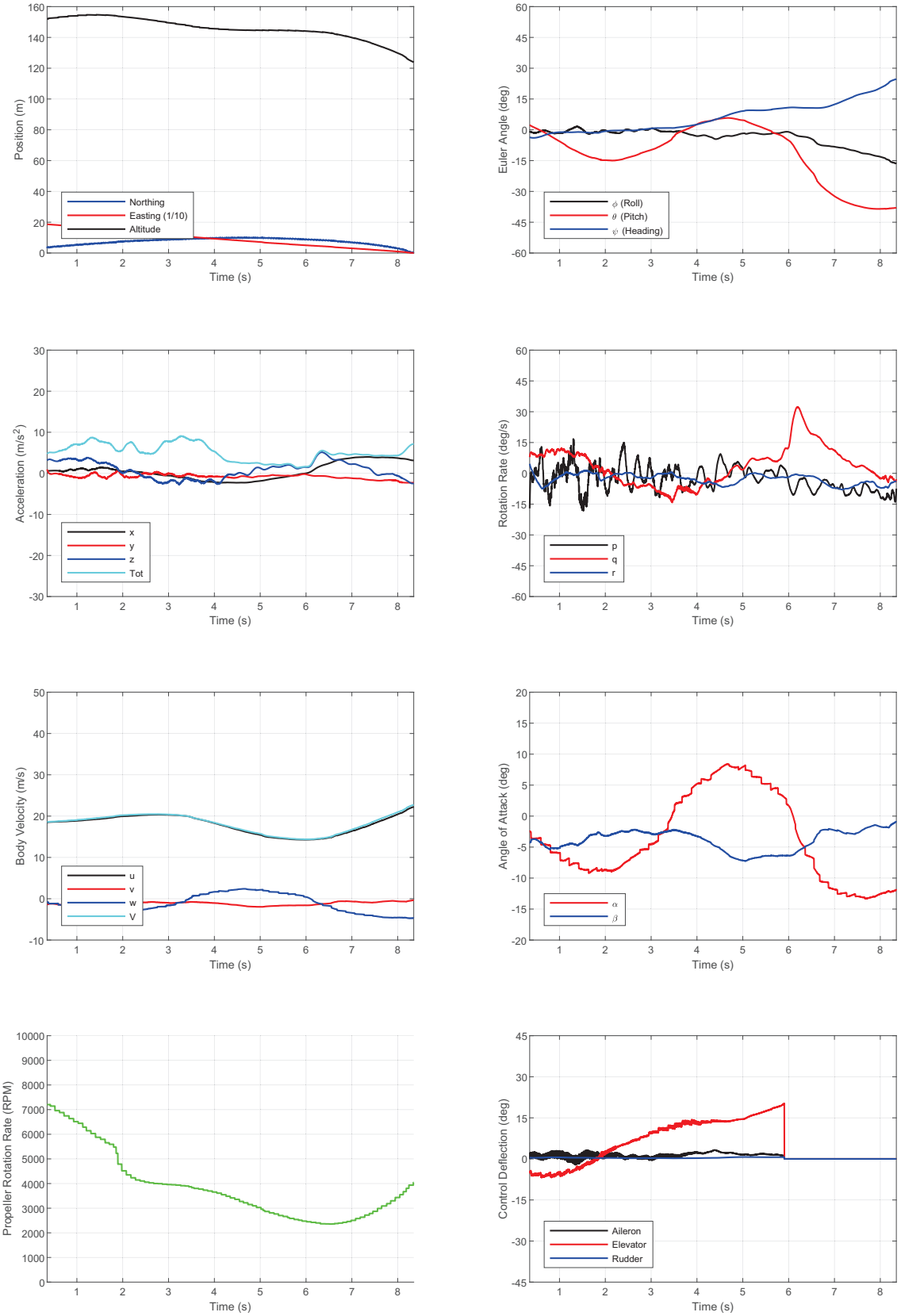

Figure 20. Time history of aircraft state during stall at 250 g greater than the standard mass.

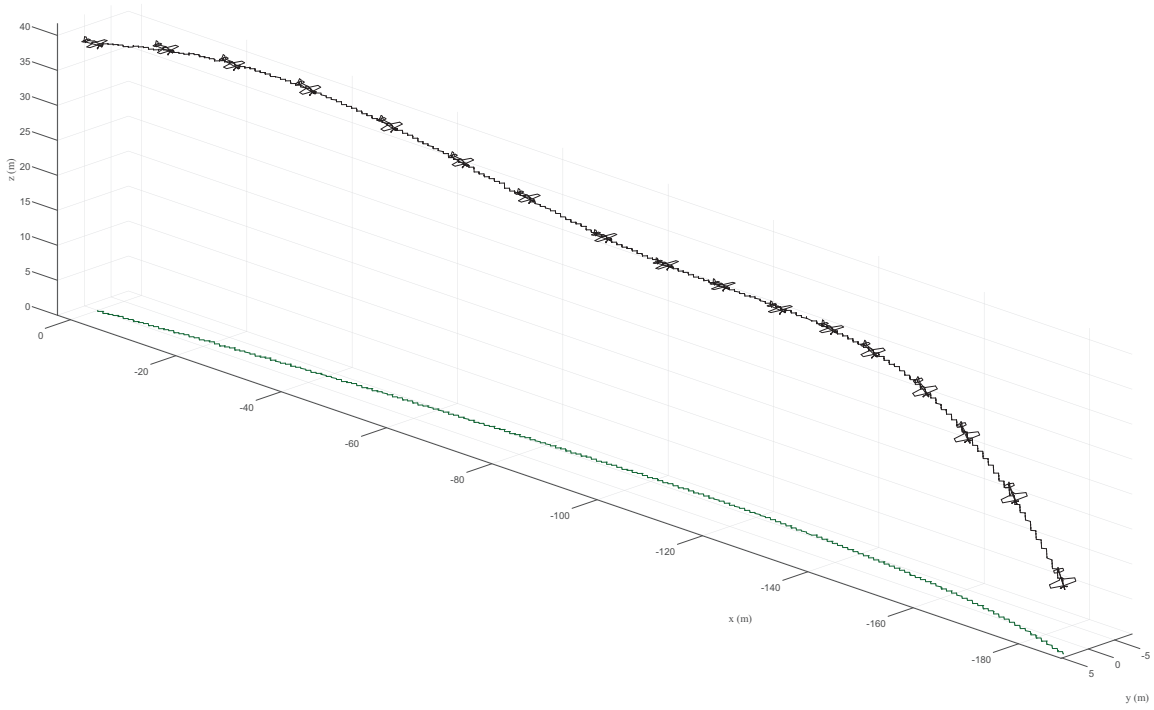

Figure 21. Trajectory of the aircraft during stall at 250 g greater than the standard mass (the aircraft is drawn once every 0.5 s)

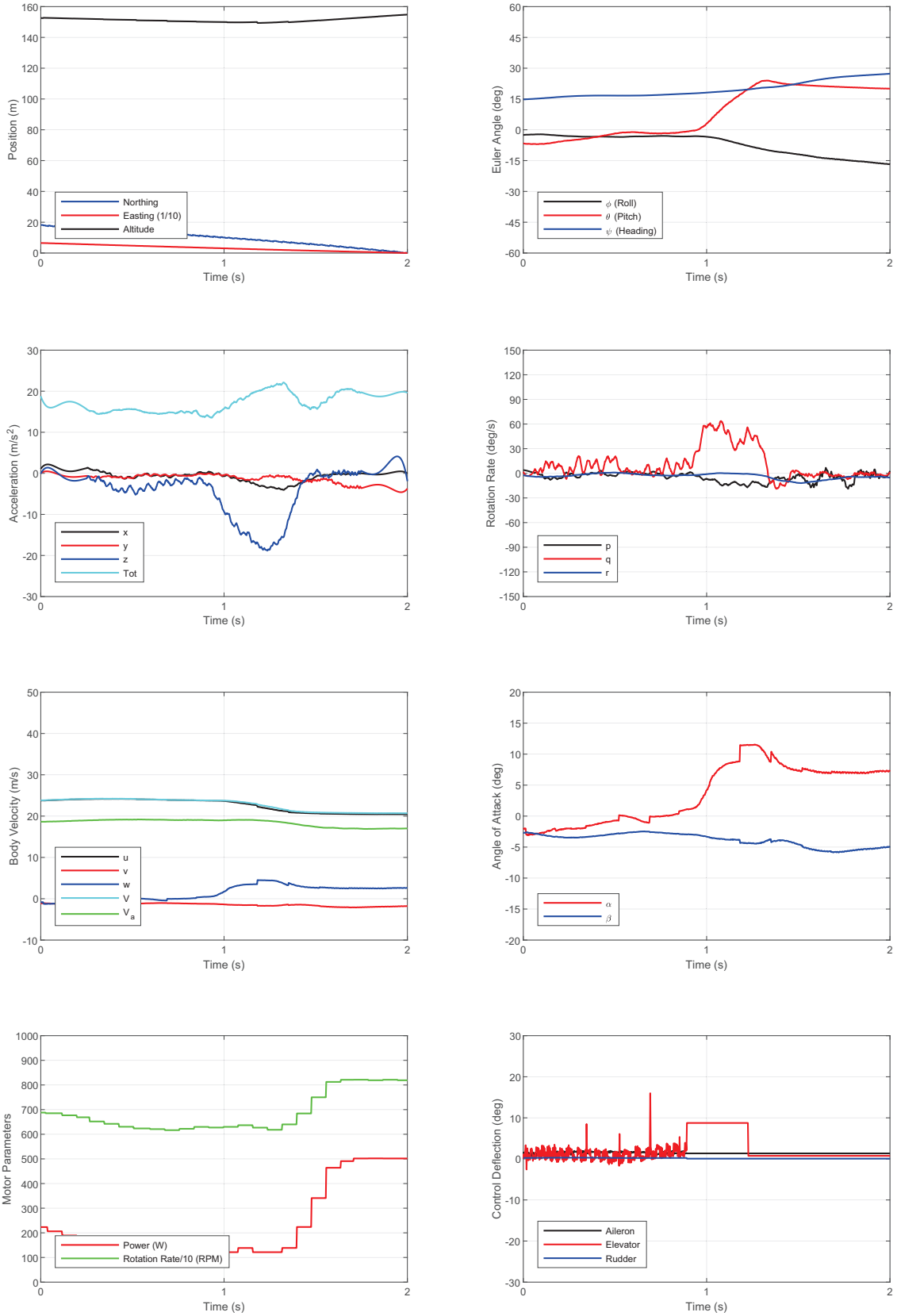

Figure 22. Time history of aircraft state during a 500 *ms*, 50% amplitude up elevator singlet.

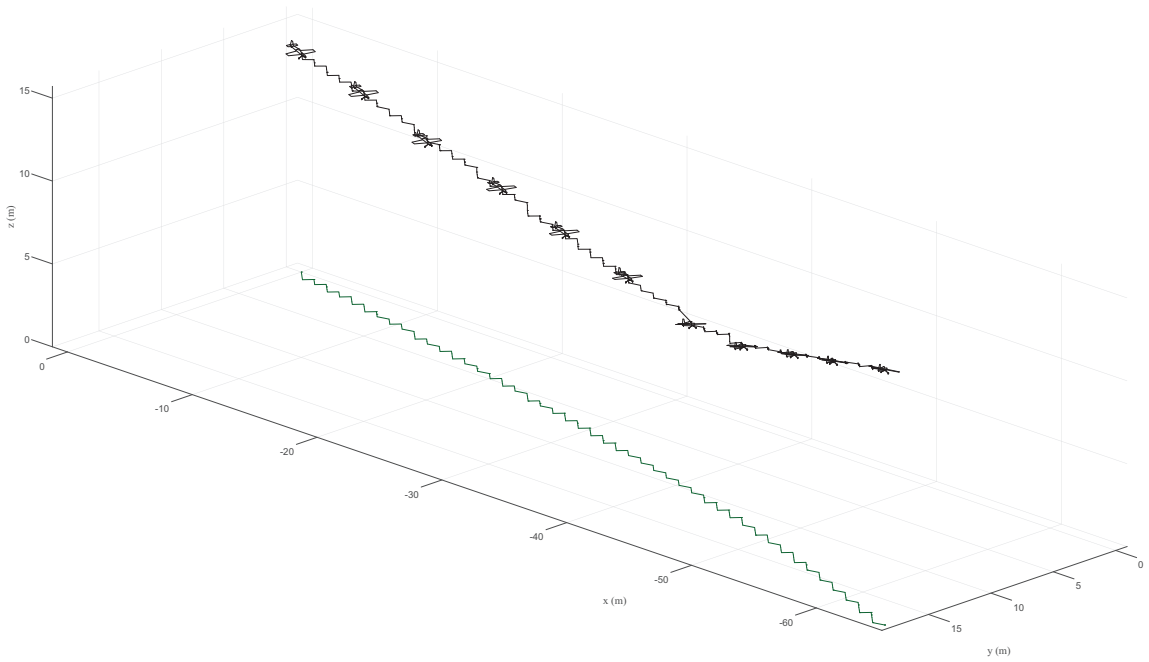

Figure 23. Trajectory of aircraft state during a 500 *ms*, 50% amplitude up elevator singlet (the aircraft is drawn once every 0.2 s).

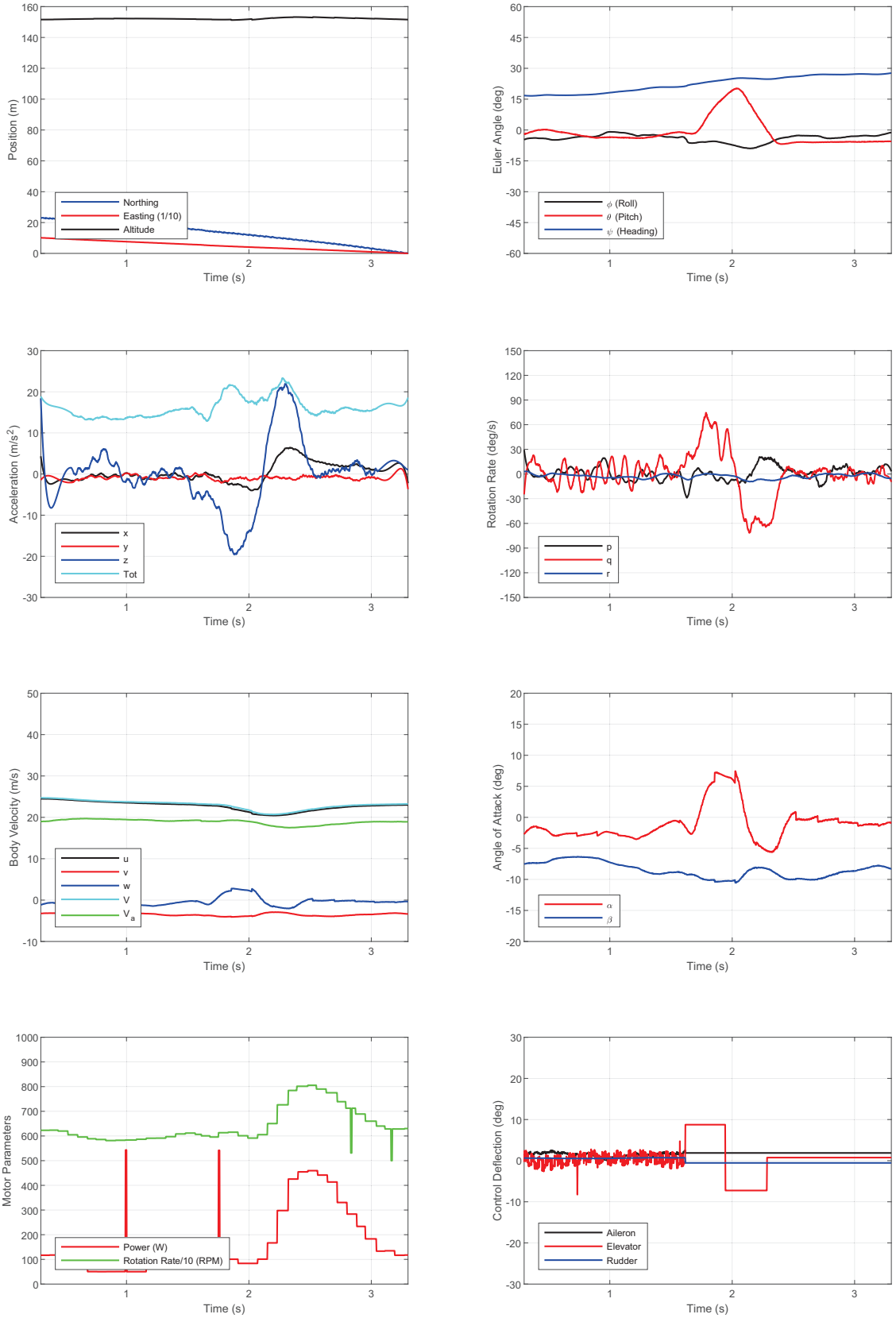

Figure 24. Time history of aircraft state during a 500 *ms*, 50% amplitude elevator doublet.

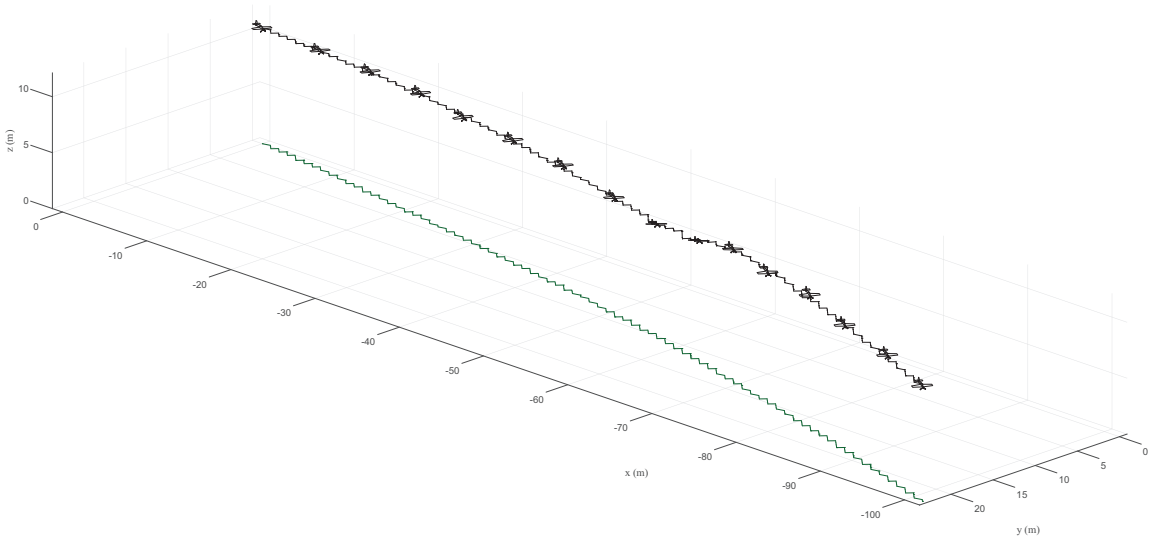

Figure 25. Trajectory of aircraft state during a 500 *ms*, 50% amplitude elevator doublet (the aircraft is drawn once every 0.2 s).

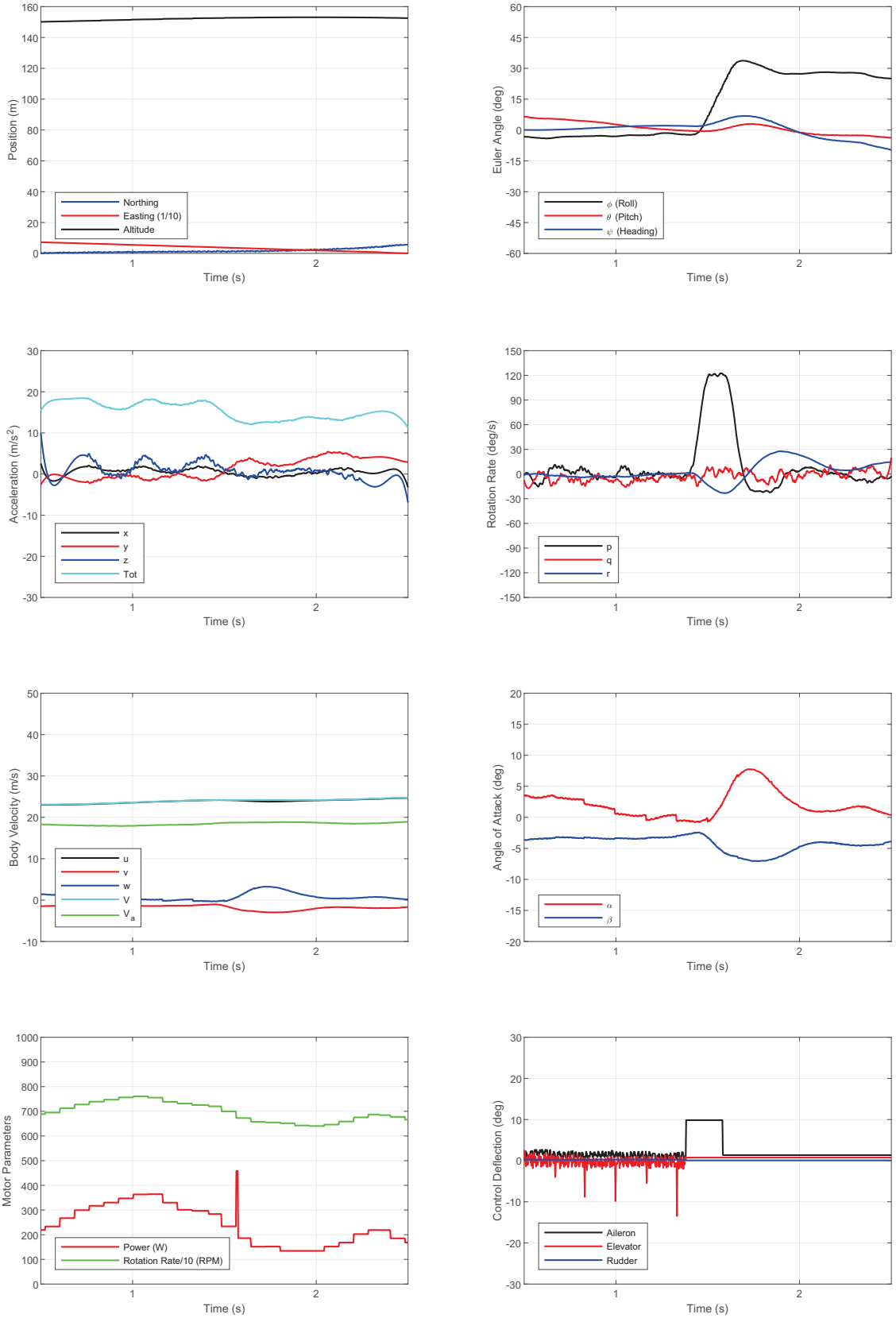

Figure 26. Time history of aircraft state during a 300 *ms*, 50% amplitude aileron right singlet.

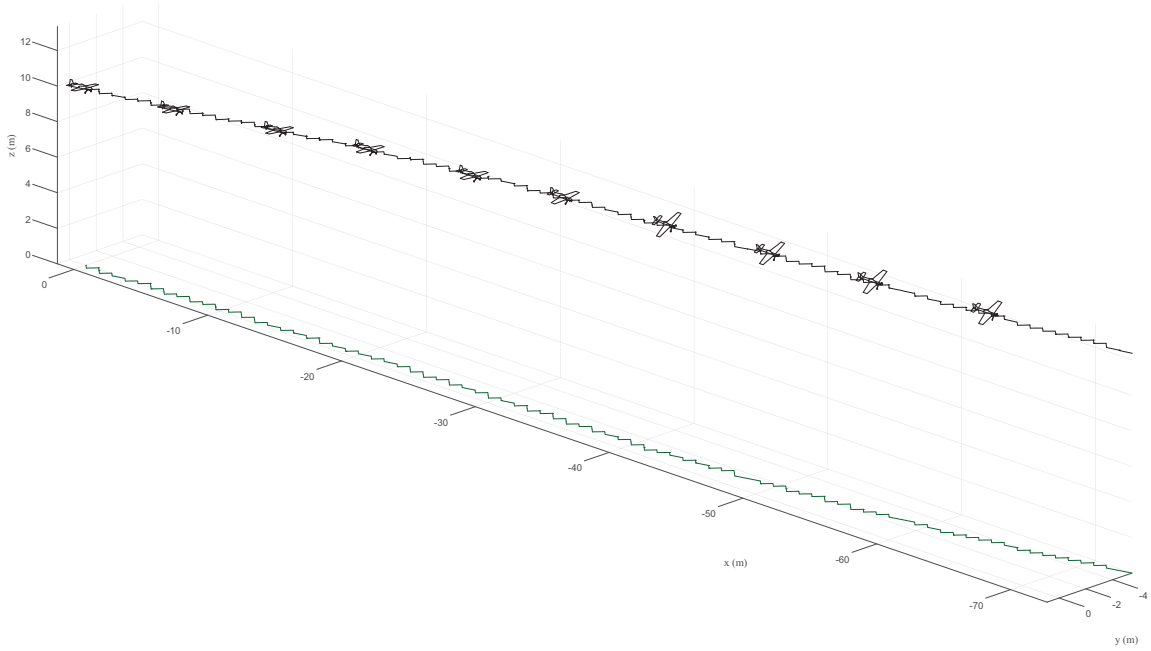

Figure 27. Trajectory of the aircraft during a 300 *ms*, 50% amplitude aileron right singlet (the aircraft is drawn once every 0.2 s).

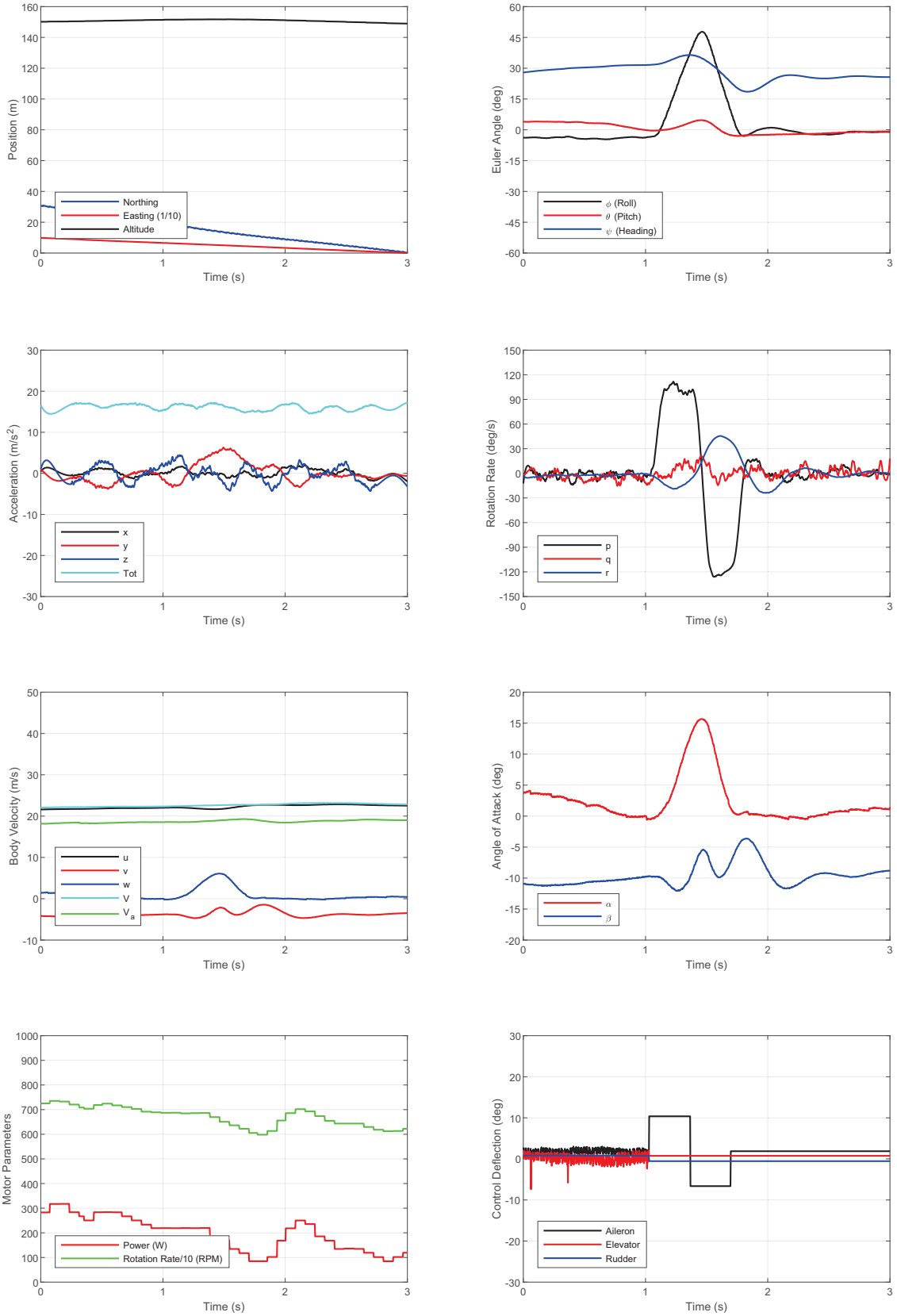

Figure 28. Time history of aircraft state during a 500 *ms*, 50% amplitude aileron right-left doublet.

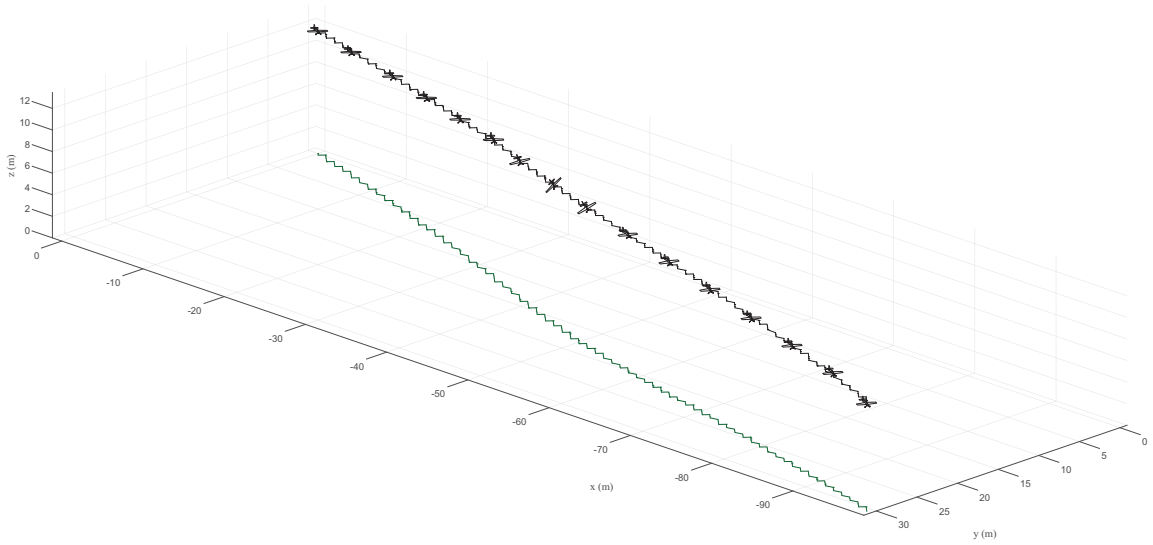

Figure 29. Trajectory of the aircraft during a 500 *ms*, 50% amplitude aileron right-left doublet (the aircraft is drawn once every 0.2 s).

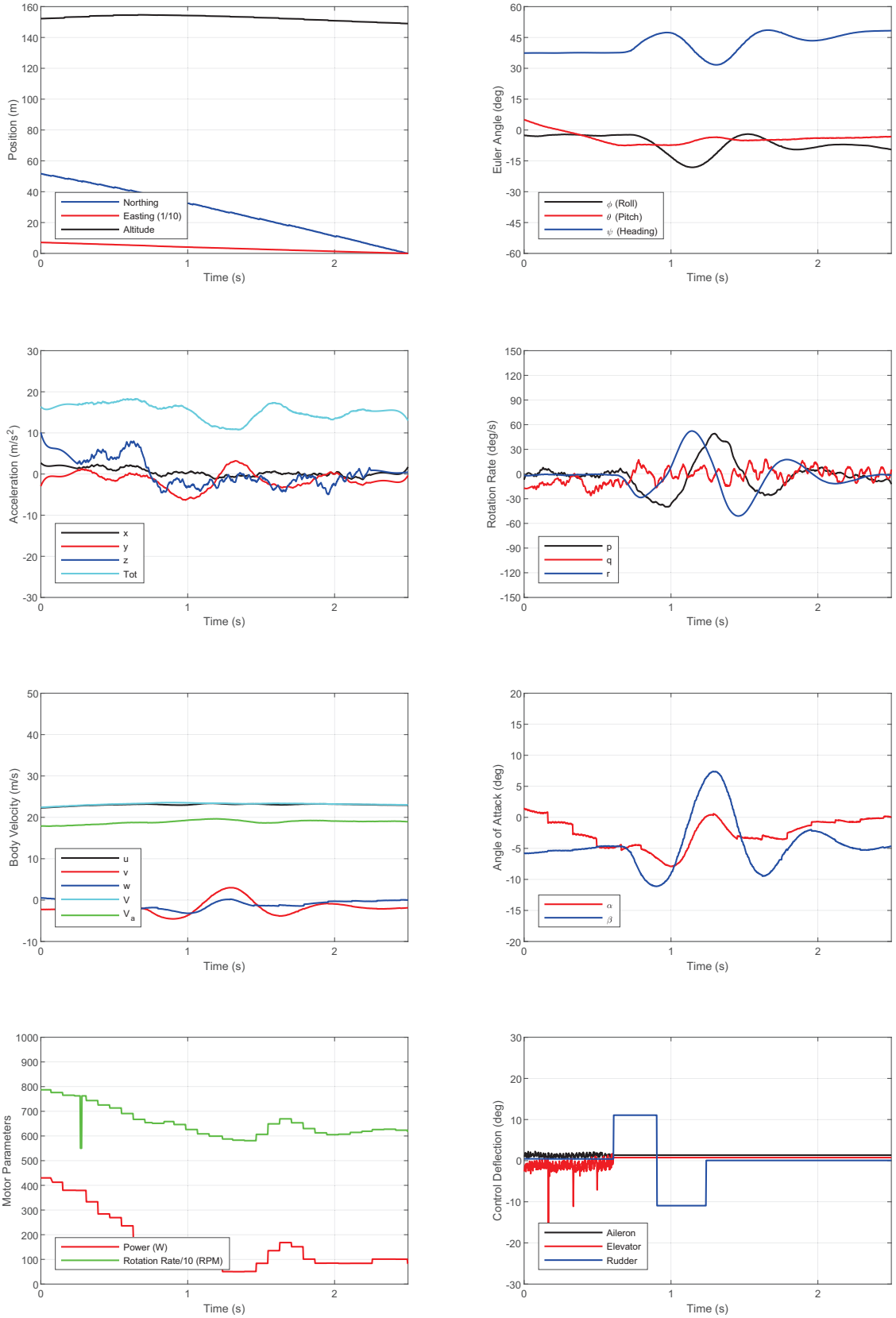

Figure 30. Time history of aircraft state during a 500 ms, 50% amplitude rudder doublet.

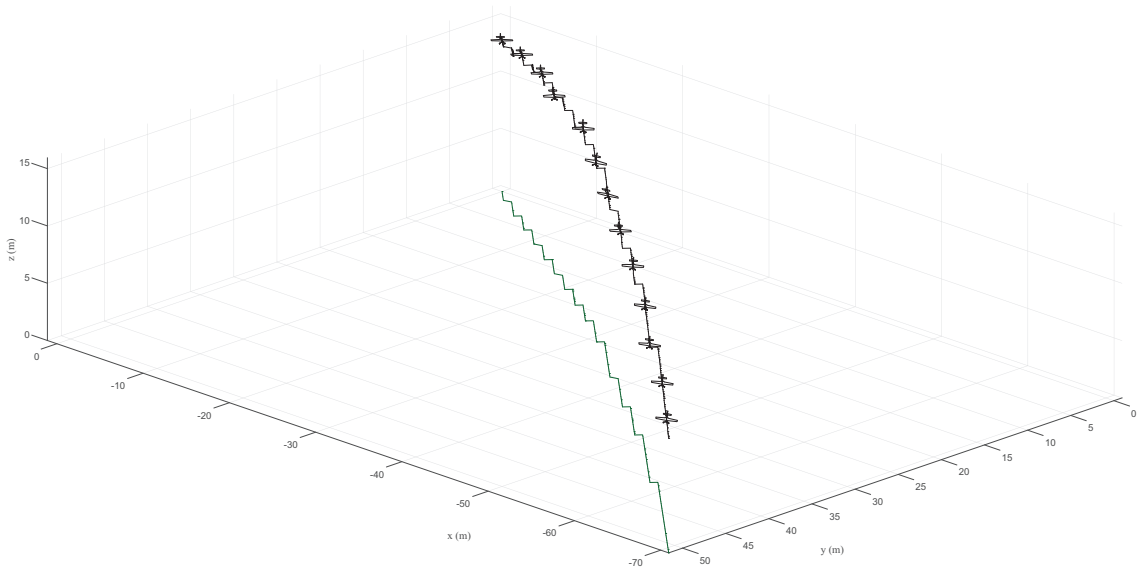

Figure 31. Trajectory of the aircraft during a 300 *ms*, 50% amplitude rudder doublet (the aircraft is drawn once every 0.2 s).